Division for Land–Ocean Ecosystem Research

- Global warming and changes in terrestrial water-material cycles in the Arctic circumpolar region
- Effects of climate change and anthropogenic forcing on the terrestrial ecosystem
- Cloud/rainfall variability in Asian monsoon regions
- Dynamics of phytoplankton in marginal seas and coastal areas
- Climate variability and changing open ocean ecosystem dynamics and biogeochemical cycle
- Interaction between oceanic waves and climate variations

The Land–Ocean Ecosystem Research Division investigates regional and global energy, water and material cycles, and physical/biogeochemical processes in the land–ocean ecosystem.

The land research group contributes to advancing our understanding of the mechanisms by which ongoing global warming and anthropogenic activity influence the terrestrial water cycle and ecosystem. Using field observations, satellite remote sensing, global meteorological data analysis, laboratory analysis, and model simulation approaches, our group aims to understand the impact of global warming on hydrological and greenhouse gas cycles in the Arctic region, the dynamics of the continental scale water cycle, the processes that drive weather and climate over Asia, the interplay between the terrestrial ecosystem and climate, and the detection of early signs of the influence of global warming in Antarctica.

Ocean research was conducted using satellite remote sensing, numerical simulations, and *in-situ* observations. We also performed synthesis studies of physical and biogeochemical processes in the ocean and their interactions with the atmosphere and climate. In particular, we are investigating how oceanic heat content, circulation, and surface waves interact with atmospheric environments and how they are linked to climate and meteorological phenomena such as tropical cyclones. We are also investigating how variations in ocean circulation, mixing processes, and air–sea fluxes influence marine ecosystems where phytoplankton are the primary producers. Moreover, we are interested in the possible impact of the marine ecosystem on physical processes and climate in the ocean and atmosphere.

Main Activities in FY2020

Estimation of clear-sky precipitation over the East Antarctica using the tritium tracer technique

In the Antarctic plateau, precipitation falling from clear skies (known as diamond dust) occurs almost daily; however, a few major synoptic events can produce a significant fraction of the annual accumulation. Thus, the contribution of clear-sky precipitation to the total accumulation on the plateau is not clear. Here, we introduced an alternative method for partitioning between synoptic and clear-sky precipitation: tritiated water (^{3}HHO). Tritium (^{3}H) is a cosmogenic nuclide that is mainly produced in the upper atmosphere of Antarctica. After ^{3}HHO generation, it follows the hydrological cycle pathway, with only small perturbations owing to the fractionation effect during phase changes. Consequently, ^{3}HHO concentrations in diamond dust formed by the condensation of local Antarctic water are characterized by higher ^{3}HHO than synoptic precipitation accompanied by moisture transported from the surrounding ocean. This is supported by the observations seen: a gradual increasing trend from the coast to the plateau region and a rapid increase in ^{3}HHO toward inland plateau

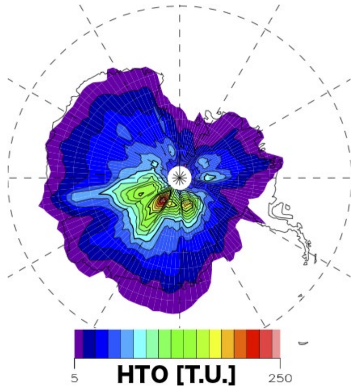

Simulated ^{3}HHO of the annual precipitation over Antarctica. A gradual increasing trend toward inland was simulated.

areas. In this study, an atmospheric circulation model incorporated into ^{3}HHO was developed to quantitatively understand the observations. A gradual increasing trend of ^{3}HHO toward the inland area was successfully simulated by the new model. The model showed that the seasonal ^{3}HHO variation was linked to the precipitation amount. The highest ^{3}HHO corresponded to a month with a weak precipitation flux. In contrast, the months with a large precipitation flux due to the frequent passage of synoptic systems were characterized by lower ^{3}HHO values.

(Reference: Kurita et al. (2020): Application of tritium tracer technique to the partitioning between clear-sky and synoptic precipitation over the Antarctic plateau, The 11th Symposium on Polar Science, on-line meeting, Nov. 16–Dec. 18, 2020)

Groundwater age of spring discharges under changing permafrost conditions: A vulnerability assessment of permafrost in the Khangai Mountains, central Mongolia

To detect the permafrost thaw and ground ice melt in the permafrost zone of Mongolia, groundwater ages of several spring discharges were determined using two transient tracers: 3H and chlorofluorocarbons (CFCs). Spring water samples were collected seasonally from 2015 to 2019 at seven spring sites around the Khangai Mountains, central Mongolia. The sites included two thermokarst landscapes on the northern and southern sides of the mountains. The 3H and CFC concentrations in the spring water in the thermokarst landscapes were very low, and the estimated mean groundwater age for these sites was older than that of the other sampled springs. Consequently, the young water ratios of the thermokarst sites were lower than those of the other springs. However, this ratio gradually increased with time, indicating that recently recharged rainwater began to contribute to the spring discharge at the thermokarst sites. An atmospheric water budget analysis indicated that the net recharge from current precipitation to shallow groundwater during the summer season was almost zero on the southern side of the mountains. Thus, spring water at the thermokarst sites on the southern side of the mountains contained large amounts of ground ice-melt water. Although long-term sampling was not performed, evidence was obtained to show that the groundwater in the region is highly vulnerable because of permafrost thaw and ground ice melt, primarily due to ongoing climate change.

(Reference: Hiyama, T. et al. (2021): Groundwater age of spring discharges under changing permafrost conditions: the Khangai Mountains in central Mongolia. *Environmental Research Letters*, 16, 015008, doi:10.1088/1748-9326/abd1a1)

Diurnal precipitation cycle in the high-elevation area over the Himalayas

The diurnal precipitation cycle is important for the hydroclimate in the Himalayas during summer. However, features of the diurnal cycle affecting precipitation from the foothills to glacierized, high-elevation areas are poorly understood. In this study, we investigated the diurnal precipitation cycle in summer using data from three years (2016–2018) of *in-situ* observations from an automatic weather station, which is close to a glacier at 4809 m asl in the Rolwaling Valley in the eastern Nepal Himalayas. We identified two daily precipitation maxima, corresponding to daytime and nighttime peaks, in the diurnal cycle of the three summers. More than 80% of the total precipitation fell with a weak intensity of < 1 mm h–1; however, it had a high occurrence frequency of approximately 50%. The daytime peak resulted from upslope flows driven by the surface heating of the slopes. These upslope flows carry moist air that cools adiabatically as it travels up the slope, promoting condensation. However, the surface meteorological variables do not explain why precipitation reached a maximum in the middle of the night, suggesting that a change in large-scale atmospheric circulation might be responsible for the nighttime precipitation peak, rather than a change in the surface meteorological variables.

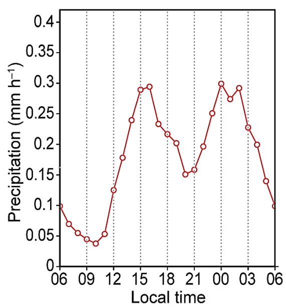

Three-year mean diurnal precipitation cycles during summer (June–September) at the automatic water station.

(Reference: Fujinami, H. et al. (2021): Twice-daily maxima of summer precipitation in high-altitude areas of the Himalayas: Two contrasting land surface effects, AGU Fall Meeting 2020, online meeting, 1–17 December, 2020)

Variation of GCOM-C Remote Sensing Reflectance in Ariake Bay using AERONET-OC data

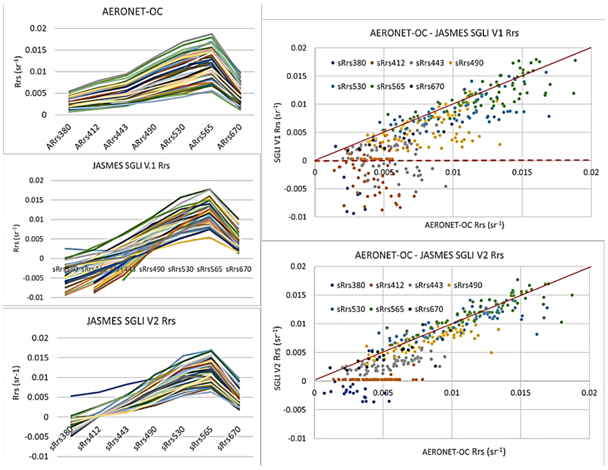

Rrs of each wavelength from AERONET-OC (left-top) and GCOM-C version 1 (left-middle) and version 2 (left-bottom), and the scattering diagrams (version 1: right-top, version 2: right-bottom).

Global Change Observation Mission-Climate (GCOM-C) was launched in December 2017, and global data of visible and infrared radiation, including ocean areas, with 250 m resolution have been accumulated. The version 2 data around Japan has been disseminated from the JAMSES (https://www.eorc.jaxa.jp/gi-bin/jasmes/sgli_nrt/index.cgi) site from June 2020. To use ocean color data, it is necessary to have frequent sea-truthing data, although this is difficult to obtain. Aerosol Robotic Network-Ocean Color (AERONET-OC) is a global network of spectral radiometers, which was modified from the radiometer developed to observe aerosols from land and sea surface radiance. For GCOM-C validation, ISEE set a JAXA-owned AERONET-OC on the Ariake Tower of Saga University in April 2018, and the data were available at the AERONET-OC site (https://aeronet.gsfc.nasa.gov/). Versions 1 and 2 GCOM-C remote-sensing reflectance (Rrs) data were verified using AERONET-OC data (see figure). Most of the AERONET-OC Rrs data peaked at 565 nm. GCOM-C Rrs data had a similar shape, although many of the Version 1 Rrs values in the 380–443 nm range were negativebecause of the absorptive aerosol in this area, which was confirmed by aerosol observations. Version 2 of Rrs (380), Rrs (412), and Rrs (443) were negative, zero, and positive, respectively, after adjustment. Version 2 Rrs was close to AERONE-OC Rrs at 490–670 nm because of this adjustment. Therefore, Version 2 Rrs was reasonably accurate at more than 490 nm, although an atmospheric correction algorithm is required to improve Rrs for short wavelengths.

Marine wave boundary layer observation using an optical particle counter with 10-Hz temporal resolution

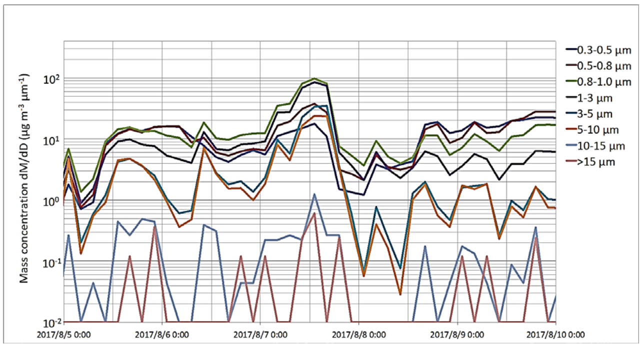

Mass concentration dM/dD (μgm^{-3}μm^{-1}) of aerosol particles before and after the passage of tropical cyclone Noru (2017) measured by an SSOPC set up at 12.5 m above the mean water level of the marine observation tower in Tanabe Bay, Wakayama Prefecture, Japan).

A sea spray optical particle counter (SSOPC) with high temporal resolution and a large sample air flow rate was developed in this study to investigate the dynamics and distribution of marine aerosols within a height of approximately 10 m from the sea surface. SSOPC measures the number of particles with eight channels in the range of 0.3–15 μm. The instrument weighs 2.5 kg and has an external dimension of 25 (H) × 17.5 (W) × 16 (D) cm. It can be mounted on a moored buoy to measure the vicinity of the sea surface or collocated with an ultrasonic anemometer on the tower of an observation vessel. In the circulation system inside the enclosure, sample and sheath air are hermetically separated from ambient air so that water does not accumulate inside the SSOPC owing to the humidity of the sample air or spray inflow. To estimate the sea salt flux by the eddy covariance, a flag signal cable to inform the operation status of the SSOPC is connected to the data logger of the ultrasonic anemometer, considering that the instrument will be installed on observation vessels in the future.

(Reference: Aiki, H., F. Kondo, M. Konda, K. Tanaka, and T. Fujita (2020): Marine wave boundary layer observation using an optical particle counter with 10-Hz temporal resolution, *Earozoru Kenkyu*, 35(3), 160–169, doi:10.11203/jar.35.160)

Mesopelagic particulate nitrogen dynamics in the subarctic and subtropical regions of the western North Pacific

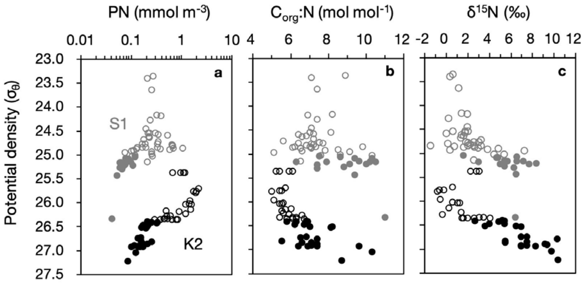

Vertical profiles of (a) PN concentrations, (b) C_{org}:N, and (c) PN-δ^{15}N of suspended particles with respect to the density anomaly σθ at K2 (47°N, 160°E: black) and S1 (30°N, 145°E: gray) stations. Open and closed circles indicate data from the surface and mesopelagic layers, respectively.

The dynamics of mesopelagic particulate nitrogen (PN) were investigated at two time-series stations in the subarctic (K2) and subtropical (S1) regions of the western North Pacific Ocean. This was undertaken during seven seasonal cruises between 2010 and 2012, where the nitrogen isotope delta (δ^{15}N) and organic carbon to nitrogen ratio (C_{org}:N) of suspended and settling particles were obtained. The suspended PN concentration was 2.2 times higher on average at K2 than at S1. Similar vertical increases in δ^{15}N by 4–5 per mil and C_{org}:N by 3–4 were found at 100–500 m at both stations, attributable to heterotrophic PN degradation. We applied these increases to a model assuming steady-state conditions for δ^{15}N to assess the degradation of the upper mesopelagic PN pool and its particle source composition. We assumed that two source particles would enter the mesopelagic pool: surface layer suspended particles (SUS0) and fragmented particles from sinking aggregates (SINK0). The relative contributions from SUS0 were estimated to be 55% and 22% at K2 and S1, respectively. The PN input by SUS0 particles was seven times greater at K2 than at S1. Efficient SUS0 particle transport at K2 was likely associated with deep (> 100 m) convective mixing over four months. In contrast, active particle recycling within the surface layer at oligotrophic S1 hindered the export of SUS0 particles. The undegraded PN fraction, f, was estimated as 0.26–0.69 and 0.34–0.76 at K2 and S1, respectively. Lower f values were estimated at K2 through the mesopelagic column, indicating that the source particles underwent greater degradation. Furthermore, 78% of the mesopelagic degradation occurred between 100 and 200 m at this station. The lower microbial degradation rate at 200–500 m is likely due to a lower oxygen concentration than that in the upper column of K2. These estimations of mesopelagic PN degradation provide insight into biological carbon sequestration in the deep sea.

Evaluation of satellite-derived global net ocean surface heat flux

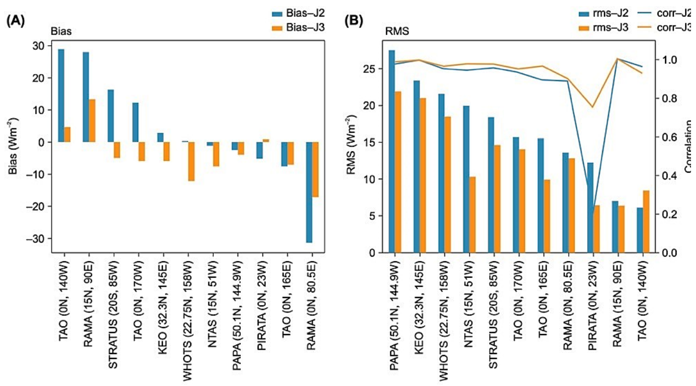

Comparison of (A) bias, (B) RMS, and correlation coefficient (lines) of J-OFURO3 V1.1 (J3) and old generation data (J2) among 11 *in-situ* buoys. Bias and RMS are in descending order based on J2.

Accurate global estimation of net ocean surface heat flux is essential for understanding the nature of air–sea interactions in the climate system. A research project on surface heat flux estimation based on satellite observation J-OFURO has released global flux data for the past 30 years using multiple satellite observation data and the development of advanced estimation technology (J-OFURO3 V1.1). The surface heat flux consists of four components (latent heat, sensible heat fluxes, and shortwave and longwave radiation), and the accuracy of each component has been evaluated so far; however, the evaluation of the net surface heat flux reliability of was insufficient. In this study, we collected data from 11 *in-situ* buoy sites by observing all four heat flux components and comprehensively evaluated the net surface heat flux. It was clarified that the average bias was only 5.8 W/m^2, and the bias variation and root-mean-square error (RMSE) were smaller than those of the old generation data.
(Reference: Tomita, H., K. Kutsuwada, M. Kubota, and T. Hihara (2021): *Front. Mar. Sci.*, doi.: 10.3389/fmars.2021.612361)